Duration of Individual Relativistic Electron Microbursts: A Probe Into Their Scattering Mechanism ... Better/shorter title?

M. Shumko[1], L.W. Blum[2], and A.B. Crew[3]

[1]NASA's Goddard Space Flight Center, Greenbelt, Maryland
[2]University of Colorado Boulder, Boulder, Colorado
[3]Johns Hopkins University Applied Physics Laboratory, Laurel, Maryland

Key Points:

- We identified relativistic microbursts observed by the SAMPEX satellite and quantified their duration
- The microburst duration is shortest at midnight and longest at noon magnetic local times.
- Whistler-mode chorus rising tone element duration has a similar trend

Corresponding author: M. Shumko, `msshumko@gmail.com`

Abstract

In this study we used the Solar Anomalous and Magnetospheric Particle Explorer to identify relativistic, > 1 MeV, electron microbursts and we quantified their duration. We found the shortest microbursts, with a median duration around 80 milliseconds, near midnight magnetic local time. Microburst duration increases through dawn and to noon magnetic local time, where the median microburst duration roughly doubles to 160 milliseconds. The increasing microburst duration trend in magnetic local time is similar to the whistler mode chorus rising tone element duration, shedding light into the microburst scattering mechanism.

Plain Language Summary

Microbursts are a naturally occurring form of electron precipitation from the near-Earth space into the atmosphere. They are characterized by their short duration, typically defined to be less than a second, or sometimes as 100 milliseconds... Microburst impact on the atmosphere includes the degradation of Mesospheric Ozone through the production of Odd Nitrogen and Odd Hydrogen molecules... We don't know the details on how microburst electrons are scattered, but there is evidence that they are scattered by whistler-mode chorus rising tone elements... Talk about duration and how it is a probe into the scattering physics.

1 Introduction

Outline

1. Introduce particle accelerating/scattering mechanism... dual role of chorus waves.
2. One manifestation of electron-chorus scattering are electron microbursts.
3. Briefly describe microbursts and their properties.
4. Mention the chorus-microburst link, but it is currently unknown the physics of how electrons get scattered. Two approaches are quasi-linear diffusion and non-linear scatterring.
5. Talk about microburst-chorus rising tone element duration and how they are similar. Mention the prior microburst width studies.
6. The microburst width has not been explored as a function of geomagnetic indices or location.
7. The trends in microburst width (duration) can be a probe into the conditions necessary to scatter microburst electrons.

2 Instrumentation

Outline

1. Describe SAMPEX
2. Describe HILT
3. Describe the 20 ms data used in this study (State4, 20 ms, avoided spin times). Data duration.

In this study we used the > 1 MeV electron count data, taken by the Heavy Ion Large Telescope (HILT) instrument CITE HERE, that was onboard the Solar Anomalous Magnetospheric Particle Explorer (SAMPEX) satellite CITE HERE.

The SAMPEX satellite was launched on X and reentered the atmosphere on Y CITE HERE. It was in a 520x670 km, 82° inclination orbit. Broadly, the SAMPEX had two

57 pointing modes: spin mode and zenith pointing modes. To avoid the compounding ef-
58 fects due to the variable pitch angles sampled in the spin mode, we focused this study
59 on the zenith pointing data.

3 Methodology

61 To estimate the microburst duration we first identified microbursts and then we
62 fit them with a Gaussian model with a linear trend to quantify the duration for each mi-
63 croburst.

3.1 Microburst Identification

65 We identified microbursts using the burst parameter defined by O'Brien et al. (2003)
66 and used in numerous other microburst studies with SAMPEX (e.g. Douma et al., 2017).
67 Assuming Poisson probability for the observed electron counts, the burst parameter is
68 the number of standard deviations of a foreground signal above the background, expressed
69 as

$$n_\sigma = \frac{N - A}{\sqrt{A + 1}} \tag{1}$$

70 Find a better variable than bp. This is not British Petroleum where N is the number
71 of foreground electron counts (microburst or otherwise), and A is the centered running
72 average background counts. The 1 in the denominator prevents a division by 0 error. In
73 O'Brien et al. (2003), and in the results in this study, N was summed over 0.1 seconds
74 and is called N_{100}, while A was summed over 0.5 seconds and is called A_{500}. Henceforth
75 we will specify the time window with the subscript for N and A. Times when bp > 10
76 are classified as microburst times, and the peak count rate in each time interval is saved
77 as a microburst to our data set. With A_{500} and N_{100}, we detected a total of 256,764 mi-
78 crobursts over the 13 year period from 1997 to 2012. Four examples of microbursts are
79 shown in Fig. 1 by the solid black curves.

80 Check the argument for clarity The choice of A determines the sensitivity of the
81 burst parameter to microbursts of various durations (widths). This sensitivity is best
82 illustrated with an example. Given a 1-second wide microburst, if we use A_{500}, the cen-
83 tered average background at the microburst time is skewed towards the microburst peak
84 and the microburst's bp is reduced, potentially below the detection threshold. On the
85 other hand, if we use A_{1000}, the centered running background will be relatively less el-
86 evated at the microburst time so it has a greater bp and is more likely to be detected.
87 In other words, *bp* will be relatively larger for A_{1000} than A_{500}. This sensitivity mani-
88 fests itself as a bias towards detecting narrower microbursts that we will address later
89 in this study.

3.2 Microburst Duration

91 We estimated the microburst duration using two methods that yielded similar re-
92 sults: the duration at half of the microburst's topographic prominence and duration from
93 a Gaussian fit.

94 The topographic prominence is a simple and robust method to estimate the mi-
95 croburst duration used to identify curtains a similar-looking type of precipitation (Shumko
96 et al., 2020) Fix citation once paper is published. It is defined as the duration at half
97 of the microburst topographic prominence: the height of the microburst relative to the
98 maximum of the two minima on either side of the microburst peak. On each side of the
99 microburst peak, the minima are searched for between the microburst and a higher peak
100 on that side. While the topographic prominence method of estimating microburst du-
101 rations is simple and robust, one of its downsides is its inability to automatically ver-
102 ify that the duration is representative of a single microburst. Therefore, we also fit mi-

SAMPEX/HILT Microburst Fits

Figure 1. Example $>$ 1 MeV microbursts shown by the black lines, and the fits shown by the dashed red lines. The fit full width at half maximum (FWHM) and the $\bar{R}^2$ goodness of fit metric is annotated in each panel. Microbursts with $\bar{R}^2 > 0.9$ were used for this study. The major time ticks are at every second, while the minor ticks are at every 100 milliseconds.

crobursts with a Gaussian, and used the R^2 goodness of fit metric to filter out bad duration estimates.

The other method that we use to estimate the microburst duration is fitting a Gaussian shape to microbursts. The advantage of this method is that it allows us to evaluate the fit using a goodness of fit metric. By screening out bad fits, we exclude superposition of multiple microbursts that will unintentionally bias our microburst duration estimate.

We assumed a Gaussian superposed with a linear trend fit model. The Gaussian models the shape of the microburst; while the linear trend accounts for the electrons that are either trapped or quasi-trapped in the drift loss cone. The fit model is defined as:

$$c(t|A, t_0, \sigma, c_0, c_1) = A e^{-\frac{(t-t_0)^2}{2\sigma^2}} + c_0 + c_1 t \qquad (2)$$

where A, t_0, and σ are the Gaussian amplitude, center time, and standard deviation; while the c_0 and c_1 are the background count intercept and slope. The fit was applied over a number of data points determined by the maximum of either: 4x topographic prominence width or 0.5 seconds. A challenge to any robust and automated nonlinear regression algorithm is guessing the initial parameters. The initial parameter guesses for the Gaussian are provided by the topographic prominence and topographic duration estimates. The two linear trend initial parameters were: $c_0 = 50$ and $c_1 = 0$. The optimal fit parameters were found using scipy's `curve_fit()` function in Python. We defined the microburst duration as the full width at half maximum (FWHM) of the microburst peak, defined as

$$\text{FWHM} = 2\sqrt{2\ln 2}\,\sigma. \qquad (3)$$

To evaluate the fit, we used the R^2 goodness of fit metric. R^2 is defined as

$$R^2 = 1 - \frac{SS_{res}}{SS_{total}} = 1 - \frac{\sum (c_i - f_i)^2}{\sum (c_i - \bar{c})^2} \qquad (4)$$

where SS_{res} is the sum of squares of the residuals between the observed counts c_i and the fit counts f_i for each time stamp, and SS_{total} is the sum of squares between c_i and the mean counts $\bar{c}$.

One interpretation of R^2 is: fractionally how much better the variance in the data is explained by the model fit, compared to the null hypothesis horizontal line at $\bar{c}$. When

129 $R^2 = 1$, the modeled fit perfectly describes the variance in the data, and R^2 can be ar-
130 bitrarily negative for poor fits (a fit can be much worse than the mean).

131 To account for overfitting that results from the variable number of data points used
132 for each fit, the adjusted R^2, $\bar{R}^2$, was used. It is defined as

$$\bar{R}^2 = 1 - (1 - R^2)\frac{n-1}{n-p-1} \tag{5}$$

133 where n is the number of data points fit, and p is the number of parameters. Intuitively,
134 $n-1$ is the number of degrees of freedom for the null hypothesis, and $n-p-1$ is the
135 degrees of freedom for the fit model. Fits with $\bar{R}^2 > 0.9$ are considered good fits and
136 are used for the rest of this analysis. We compared the microburst duration estimated
137 with the prominence and fit methods. With the $\bar{R}^2 > 0.9$ constraint, we found that for
138 85% of microbursts, the duration estimated by both methods agreed to within 25%.

139 Figure 1a shows an example of two superposed microbursts that had a fit $\bar{R}^2 =$
140 0.83 that were excluded from this study. On other hand, Fig. 1b-d show microbursts that
141 were included in this study because the fit $\bar{R}^2 > 0.9$.

142 Lastly, Fig. 1c,d demonstrate the necessity of the linear fit to account for the chang-
143 ing background. The linear fit accounts for the non-zero mean background counts and
144 the different amplitudes of the edges of the Gaussian. Of the 256,764 detected microbursts,
145 109,231 had $R^2 > 0.9$ and are used for the remainder of this study.

4 Results

147 The well-fit microbursts are used to quantify the distribution of microburst dura-
148 tion (FWHM) for all microbursts, as a function of L and MLT, and as a function of the
149 Auroral Electroject (AE). We begin with the overall microburst distribution.

150 Figure 2 shows the distribution of all well-fit microbursts. This distribution is peaked
151 with the median at 98 ms and quickly drops off. The interquartile range spans about a
152 factor of two in microburst duration, from 67 to 140 ms.

153 Figure 3 shows the joint distribution of microburst duration as a function of L and
154 MLT. Figure 3a-c show the 25%, 50%, and 75% percentiles of microbursts in each L-MLT
155 bin. The sparse bins with less than 100 well-fit microbursts are white. For reference, Fig.
156 3d shows the number of well-fit microbursts observed as a function of L and MLT.

157 In Fig. 3, the microburst duration trend is almost identical for the different per-
158 centiles, but lets focus on the median distribution, Fig. 3b. In MLT, the median microburst
159 duration increases by a factor of two: from 80 ms at midnight to 160 ms at noon. In L-
160 shell, the median microburst duration slightly increases with L shell, most apparent near
161 midnight MLT. To disentangle the L and MLT distribution, Fig. 4 shows the marginal-
162 ized distributions; MLT was marginalized out in Fig. 4a and L-shell was marginalized
163 out in Fig. 4b. Figure 4a shows a slight broadening of the microburst duration at higher
164 L-shells; in contrast to Fig. 4b that clearly shows that the microburst duration increases
165 from midnight to noon MLT.

166 Lastly, we investigated the dependence of microburst duration as a function of ge-
167 omagnetic activity. To be consistent with the prior wave and microburst studies, we use
168 the Auroral Electrojet (AE) index to quantify the level of geomagnetic disturbance. We
169 adopt the same three AE intensity levels used in prior studies, such as Li et al. (2009),
170 Douma et al. (2017), and Meredith et al. (2020): AE < 100, 100 < AE < 300, and
171 300 < AE < 1000, in nanotesla units. Figure 5 shows the distribution of microburst
172 duration as a function of AE. This distribution is similar across the three AE intensity

Distribution of > 1 MeV Microburst Duration
SAMPEX/HILT
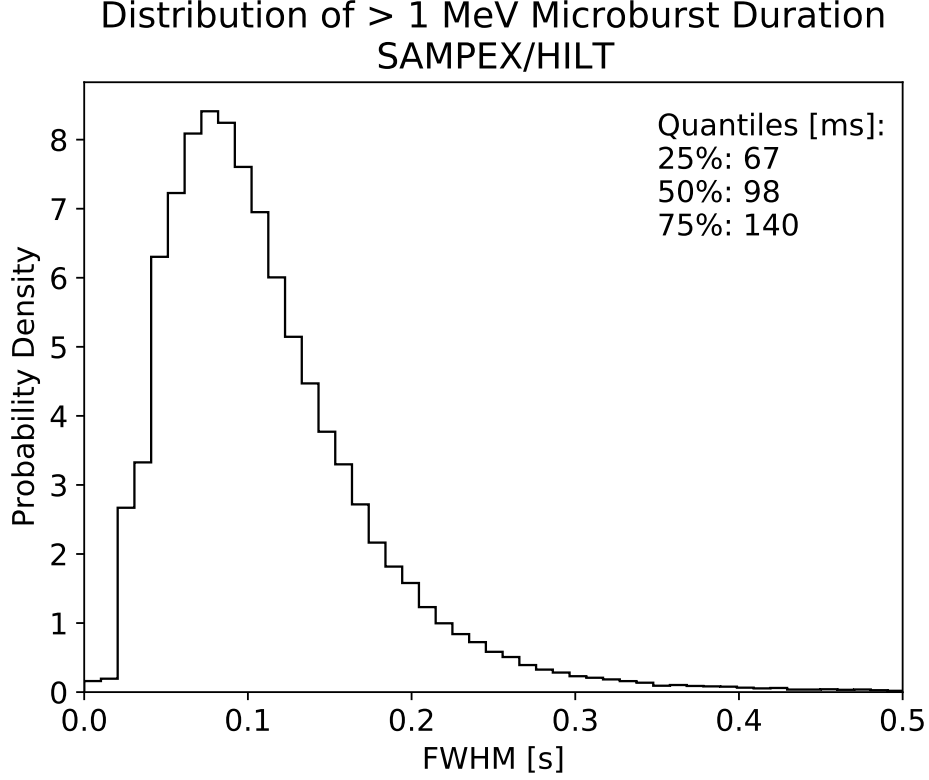
Figure 2. The distribution of all microburst full width at full maximum (FWHM).

¹⁷³ levels. However, the distribution is more prominently peaked at 0.1 s at the highest in-
¹⁷⁴ tensity level.

5 Discussion and Conclusions

Outline

¹⁷⁷ 1. Compare to prior microburst width estimates.
¹⁷⁸ 2. Comment that microbursts at lower energy are wider (data + model). The cited
¹⁷⁹ microburst widths are dependent by the energy channel of the instrument.
¹⁸⁰ 3. Compare to chorus rising tone element duration trends.
¹⁸¹ 4. A few concluding remarks.

¹⁸² To address the burst parameter preferential bias to narrower microbursts, as in-
¹⁸³ troduced in section 3.1, we ran the microburst identification algorithm on the data us-
¹⁸⁴ ing three background values: A_{500}, A_{1000}, and A_{1000}. As described in section 3.1, an de-
¹⁸⁵ tection algorithm who's centered running average is over wider time periods will be more
¹⁸⁶ sensitive to wider and less prominent microbursts. Therefore we can identify the bias if
¹⁸⁷ there is a relative excess of longer duration microbursts when the average time was in-
¹⁸⁸ creased. We found no such excess for microburst data sets that were made using A_{1000},
¹⁸⁹ and A_{1000}. Therefore, we believe that > 1 MeV microbursts are truly narrower than 250
¹⁹⁰ ms and the A_{500} is adequate to identify > 1 MeV microbursts.

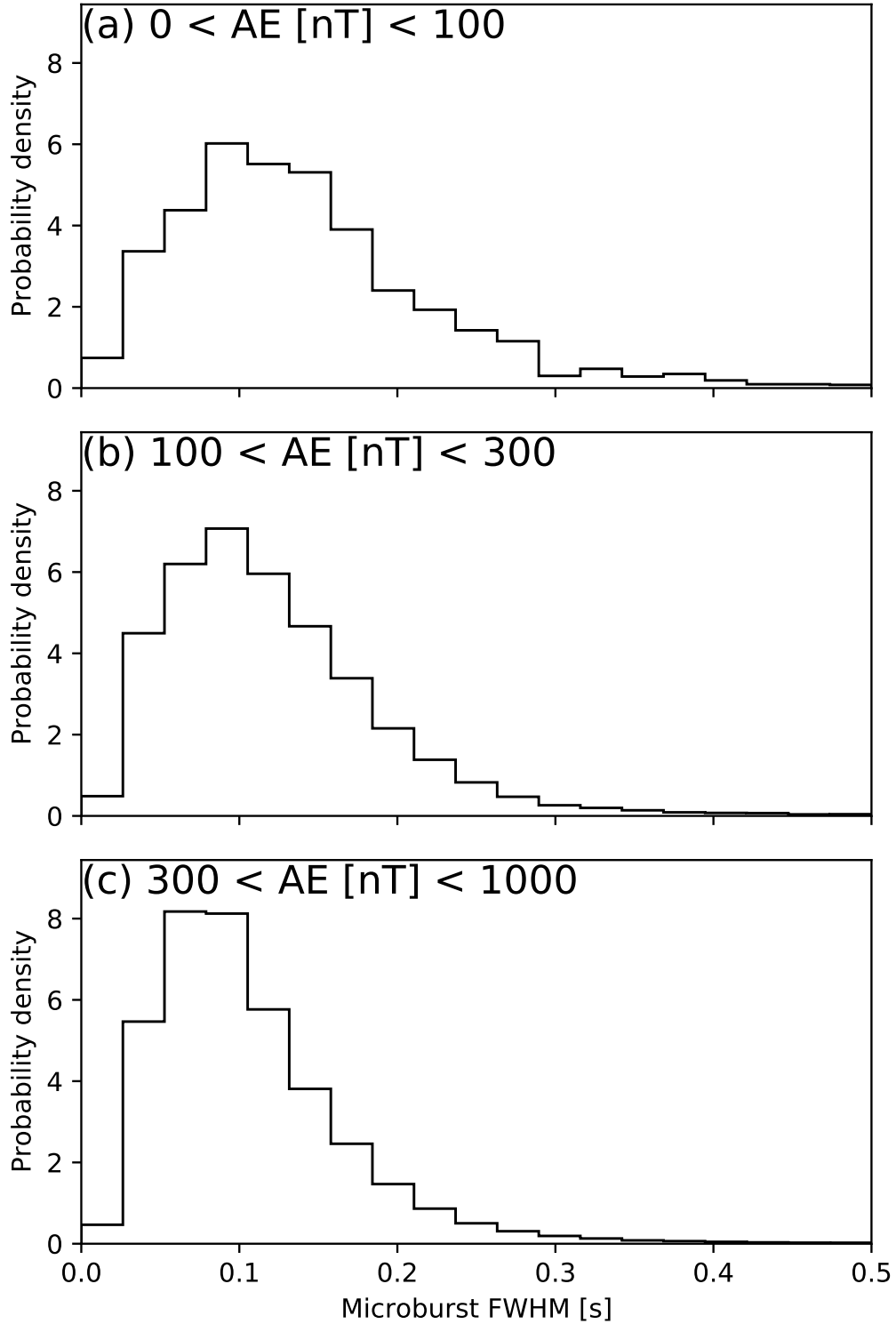## Distribution of SAMPEX microburst durations in L-MLT
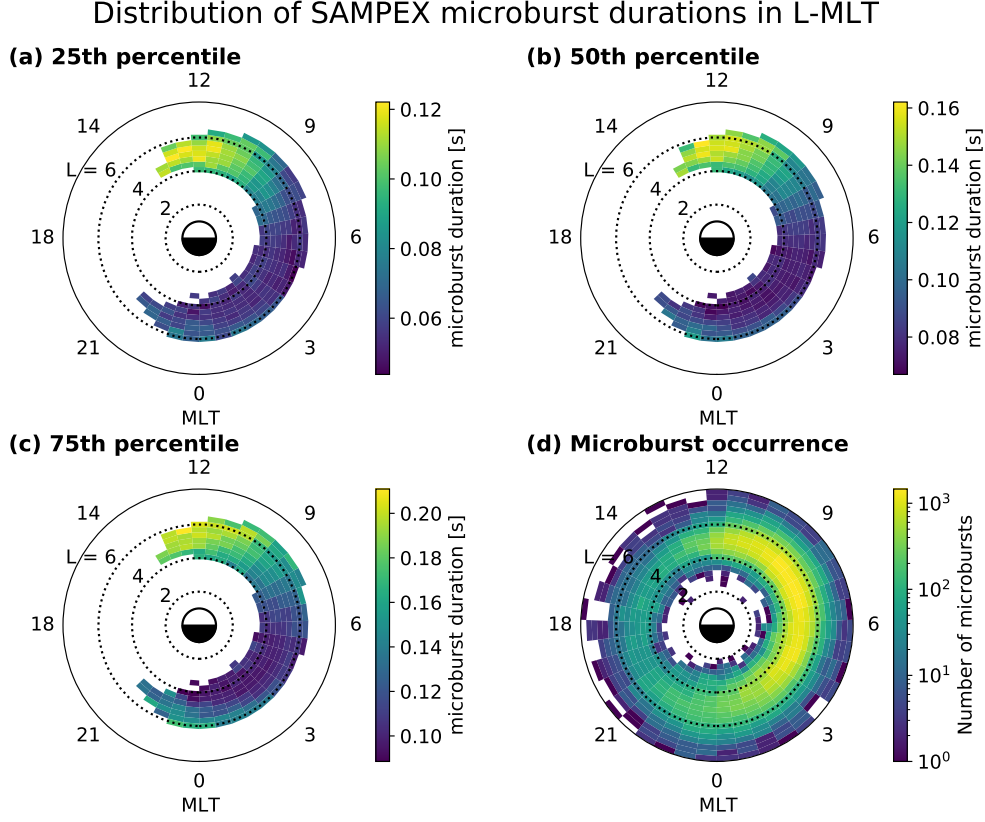
Figure 3. The joint distributions of microburst duration (FWHM) as a function of L and MLT. In each L-MLT bin with more than 100 good microburst fits, the 25th, 50th, and 75th percentiles of the duration were calculated and shown in panels a-c, respectively. The white bins in panels a-c have less than 100 good microburst fits. Panel d shows the distribution of the number of microbursts with 0 microbursts shown with the white bins.

Distribution of SAMPEX microburst durations in L and MLT
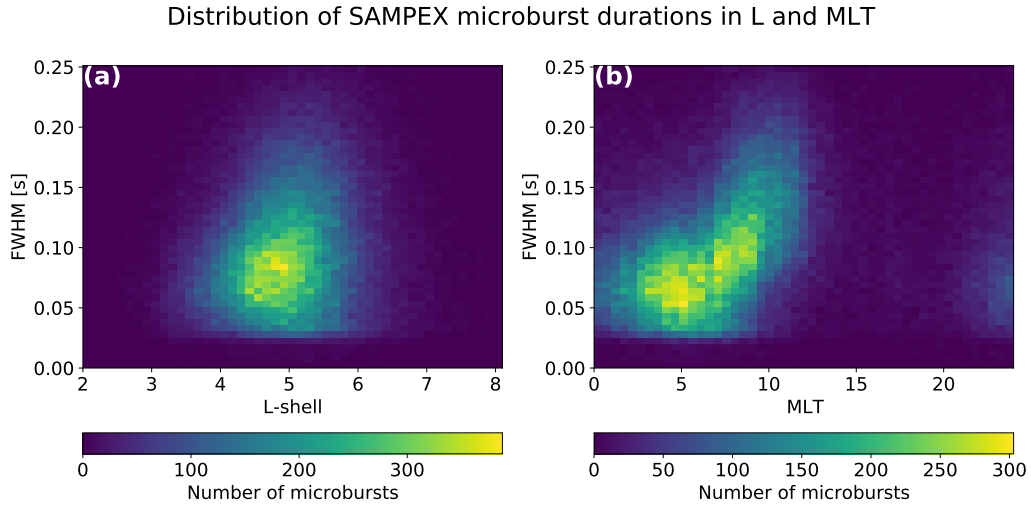
Figure 4. The marginalized distributions of the number of microbursts as a function of microburst duration (FWHM) and L shell in panel a and MLT in panel b.

Distribution of >1 MeV microburst duration as a function of AE

Figure 5. The distribution of the microburst duration (FWHM) for three ranges of the Auroral Electroject: AE < 100, 100 < AE < 300, and 300 < AE < 100 nT in Panels a-c, respectively. The x- and y-axis share identical limits between the three panels.

Acknowledgments

References

Douma, E., Rodger, C. J., Blum, L. W., & Clilverd, M. A. (2017). Occurrence characteristics of relativistic electron microbursts from SAMPEX observations. *Journal of Geophysical Research: Space Physics*, *122*(8), 8096–8107. Retrieved from `http://dx.doi.org/10.1002/2017JA024067` (2017JA024067) doi: 10.1002/2017JA024067

Li, W., Thorne, R. M., Angelopoulos, V., Bortnik, J., Cully, C. M., Ni, B., . . . Magnes, W. (2009). Global distribution of whistler-mode chorus waves observed on the THEMIS spacecraft. *Geophysical Research Letters*, *36*(9). Retrieved from `http://dx.doi.org/10.1029/2009GL037595` (L09104) doi: 10.1029/2009GL037595

Meredith, N. P., Horne, R. B., Shen, X.-C., Li, W., & Bortnik, J. (2020). Global model of whistler mode chorus in the near-equatorial region ($|\lambda_m| < 18°$). *Geophysical Research Letters*, *47*(11), e2020GL087311.

O'Brien, T. P., Lorentzen, K. R., Mann, I. R., Meredith, N. P., Blake, J. B., Fennell, J. F., . . . Anderson, R. R. (2003). Energization of relativistic electrons in the presence of ULF power and MeV microbursts: Evidence for dual ULF and VLF acceleration. *Journal of Geophysical Research: Space Physics*, *108*(A8). Retrieved from `http://dx.doi.org/10.1029/2002JA009784` doi: 10.1029/2002JA009784

Shumko, M., Johnson, A. T., O'Brien, T. P., Turner, D. L., Greeley, A. D., Sample, J. G., . . . Halford, A. J. (2020). Statistical properties of electron curtain precipitation estimated with aerocube-6. *Journal of Geophysical Research: Space Physics*, *n/a*(n/a), e2020JA028462. Retrieved from `https://agupubs.onlinelibrary.wiley.com/doi/abs/10.1029/2020JA028462` (e2020JA028462 2020JA028462) doi: https://doi.org/10.1029/2020JA028462